Influence of Deposition of rGO-TiO_2 and rGO-SiO_2 Films Order on the Properties of Electron Transport Layers

Kwanruthai BUTSRIRUK *

College of Engineering, Xi'an International University, Xi'an 710077, China

http://doi.org/10.XXXX/j01.xxxxxxx

Received 6 October 2025; accepted 28 January 2026

The titanium dioxide (TiO_2) film has been the first consideration of the electron transport layer (ETL) production for perovskite solar cells (PSCs) using a dip procedure. In which TiO_2 layer has outstanding properties like the potential of injecting electrons between layers and stability. However, the intrinsic free electrons lost still happen on the ETL. To enhance the electrical properties of ETL, rGO was incorporated into TiO_2 (Tr) and SiO_2 (Sr), where this Sr layer is another ETL layer to form an electron transport dual-layer through optimized order deposition. In this work, the conductivity values of 4 different conditions were evaluated to select the suitable ordered fabrication of a dual-layer. Encouraging, the Tr/Sr dual-layer along with using duration in dipping step (denoted as Tr/(Sr+dip)), reaching the changing of the band gap energy (E_g), and larger grain size gained up to 15.95 nm, this certain reason might significantly ascribe boosting conductivity of ETL gained up to 604×10^{-4} S/cm, including evidence from the reduced strain in the ETL lattice to 0.053. Eventually, this work revealed that the synergistic production of TiO_2 and SiO_2, with further incorporation of rGO into each ETL on a dual-layer, enables enhanced electrical properties, which is beneficial to the improvement of solar application quality in the future.

Keywords: titanium dioxide, silicon dioxide, reduced graphene oxide, conductivity, strain.

1. INTRODUCTION

Perovskite solar cells (PSCs) have been widely researched to develop the photovoltaic field. Typically, the PSCs consist mainly of an n-type semiconductor layer, also known as the electron transport layer (ETL), an intrinsic layer (i-type or perovskite layer), and a p-type semiconductor layer, also known as the hole transport layer (HTL) [1]. Expectation of optimization of PSCs performance has been studied with several technologies, improvements on ETL to generate electrons and enhance electron transport on the perovskite device, particularly [2]. To induce the ETL on the PSC, attaining a low resistance route of electron mobility or high charge mobility is required due as this layer is close to the electrode (e.g., gold (Au), silver (Ag), aluminum (Al), indium-doped tin oxide (ITO), floride-doped tin oxide (FTO), and so on), and the perovskite layer [3]. Furthermore, the lowest unoccupied molecular orbital (LUMO) of ETL should be close to the LUMO of the perovskite layer and the electrode to decrease electron-hole pair recombination, thereby reinforcing charge transfer, which is called energy level matching [4]. Several researchers refer to the versatility of ETLs, these of tungsten disulfide (WS_2), cuprous oxide (Cu_2O), ceric dioxide (CeO_2), indium-gallium-zinc-oxide (IGZO), PCBM, titanium dioxide (TiO_2), tin dioxide (SnO_2), zinc oxide (ZnO), nickel oxide (NiO), etc. These electron transport materials are extensively studied to garner a higher quality of ETLs, which leads to improved power conversion efficiency (PCE) on PSCs [5]. Specifically, titanium dioxide (TiO_2) has been applied as ETL in PSCs, which has been widely reported and studied by many research groups, due to the critical merits of TiO_2 thin films, for example, increasing the injection of electrons between layers, enhancing stability, reducing reflection, and improving light absorption [6, 7]. Conversely, the electrical properties of TiO_2 film still have a problem involving the intrinsic free electrons lost, leading to the conductivity being mitigated to less than 10^{-7} S/cm at room temperature for pristine TiO_2 film [8]. To address the low conductivity in a TiO_2 film, silicon dioxide (SiO_2) is introduced as another kind of ETL to synergize with TIO_2 to form a dual-layer ETL film for enhancing conductivity in this work [9]. Since SiO_2 has a low refractive index similar to TiO_2 and acts as an ETL when doped with certain significant material, it synergizes with TiO_2 through suitable energy level matching. Furthermore, the SiO_2 layer acts as a buffer layer or passivation layer to resist reaction with the next layer fabrication [10]. The optical property of the TiO_2 layer can show absorption of the phonon energy in the wavelength range from 290 to 400 nm [11], while the absorption of the phonon for a SiO_2 layer is in the range of 337 to 341 nm [12]. Nevertheless, the electrical properties of dual layers between TiO_2 and SiO_2 might have flaws due to the low electric conductivity of $< 10^{-7}$ S/cm on the pristine SiO_2 layer still appearing [13]. Consequently, a suitably arranged deposition for a dual-layer fabrication was further required to improve conductivity. Besides, the reduced graphene oxide (rGO) is incorporated into a dual-layer to enhance the conductivity property [14]. Due to rGO having the unique potential to suppress the coupling of electron and hole, leading to enabling boosting the electrical properties by using incorporating it into the main materials [15].

* Corresponding author; K. Butsriruk
E-mail: *Xaiu24208@xaiu.edu.cn*

Preparation of rGO-incorporated ETL on the fluoride-doped tin oxide (FTO) glass substrates has been suggested using abundant approaches, such as spin coating, sol-gel, spraying, evaporation, dipping, chemical bath deposition (CBD), etc. [16]. In the example case, the production of an ETL via spin coating has been reported to not be sufficient for obtaining a uniform film surface when compared with the dipping method, affecting the reduced electrical conductivity property [17].

Thus, the dip coating is selected as a facilitating method for fabricating ETL and an effortless process for covering a substrate of 1 × 1 cm². In this work, the order of deposition of rGO-incorporated TiO_2 and SiO_2 was assessed within the same duration in the dipping process to determine the optimal specimen for producing a dual layer on ETL.

The investigations of all specimens have been considered in the fields of optical properties, electrical properties, and morphological properties using a ultraviolet–visible (UV-Vis) spectrophotometer, a Hall-effect equipment, and an X-ray diffraction (XRD) technique, respectively [18].

2. EXPERIMENTAL PROCEDURE

2.1. Preparation of ETLs

Fluoride-doped tin oxide (FTO, TEC7, 7 ohm/sq) glass substrate was cleaned with deionized (DI) water, acetone (merck, purity ≥ 99.5 %), and ethanol (merck, purity ≥ 99.9 %), respectively, before being used as a substrate for depositing ETLs. TiO_2 (titanium (IV) oxide, aeroxide (R) P25, purity ≥ 99.5 %) and SiO_2 (nanopowder, amorphous, purity > 98.5 %) powders were dispersed in 1 m of ethanol with the weights of 7.98×10^{-2} g and 6.09×10^{-2} g, respectively. After incorporating rGO into the TiO_2 and SiO_2 solutions, they are designated as Tr and Sr, respectively. In this work, 4 different conditions for ETL fabrication were evaluated by analyzing the sequence of deposition on the FTO glass substrate with duration of 60 seconds in the dipping step (marked as dip) and without duration in the dipping step for both a single layer and a dual- layer, wherein a single layer referred to a Tr and Tr+dip layer, and a dual-layer referred to Tr followed by Sr (marked as Tr/Sr), and Tr followed by Sr+dip (marked as Tr/(Sr+dip)), respectively, as illustrated in Fig. 1.

a b c d

Fig. 1. The 4 different real experiment specimens: a – Tr; b – Tr + dip; c – Tr/Sr; d – Tr/(Sr + dip)

Actually, these 4 different conditions have been selected and considered, because without flakiness, breakage, and peeling of ETL on FTO. After the dipping step was finished, specimens were placed on a hot plate at 100 °C for 10 minutes to remove residual solvent, and then moved to a heat furnace at 500 °C for 60 minutes to form ETL. Lastly, keep all samples out of the furnace to cool down to room temperature, as shown in Fig. 2.

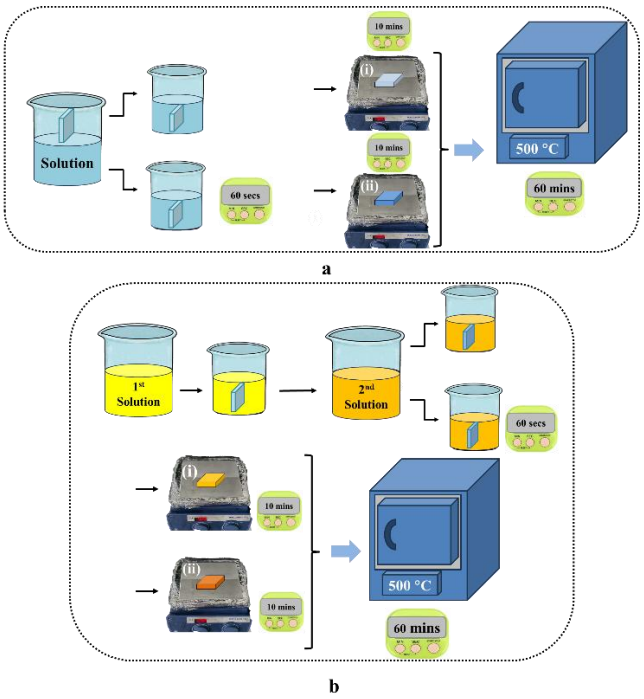

Fig. 2. The illustration of ETL fabrication by the dipping method for: a – a single layer: i – Tr; ii – Tr + dip; b – a dual-layer: i – Tr/Sr; ii – Tr/(Sr + dip)

2.2. Characterization of ETL

The elucidation of the ETL properties can be presented using various techniques. For example, the optical property was observed by determining the light absorption edge using the UV-vis spectrophotometer (Genesys 50/150/180). The electrical property of a sample size of 1 × 1 cm² was evaluated with key parameters, such as conductivity (σ), resistivity (ρ), charge mobility (n), and charge carrier concentration (μ), which was implied from the Hall Effect measurement (Linseis HCS 1) at room temperature, ultimately, the identify and analyze phases of each ETL were achieved using the measurement of the XRD technique (the Rigaku X-ray diffraction meter Miniflex600, with Cu target, the wavelength (λ) of 1.54 Å, and 2θ is in the range of 10° to 60°).

2.3. Evaluation of ETL properties

2.3.1. The band gap energy (E_g) calculation

The light absorption edge from the light transmission graph can be calculated to assess the band gap energy (E_g) from the equation of $E_g = hc/\lambda$, where h is Planck's constant of 6.63×10^{-34} J·s, c is defined as the light speed of 3×10^{-8} m/s, and λ is the wavelength [19].

2.3.2. The crucial parameters to explain the electrical property

The electrical property is a pivotal key factor to indicate the ETL performance, regarding parameters like conductivity (σ), charge mobility (n), resistivity (ρ), and charge concentration (μ). These significant parameters are obtained using the Hall-effect equipment. Whereby the σ is estimated using the following fundamental formula: $\sigma=(L/V)\cdot(l/A)$, where V is defined as the voltage, l is referred

to as the distance between each probe (in this work, the specimen has a size of 1 × 1 cm^2), and A is the area of the cross-section of the specimen [20]. In addition, the σ can be calculated from the equation: $\sigma=1/\rho=R_HA/L$, wher R_H is the sheet resistance [21].

2.3.3. The grain size and lattice distortion

The information from an XRD measurement can be used to calculate the grain size (D) of the material [22]. The computation of the D can be evaluated from relation between the full width at half maximum of the diffraction peak (FWHM, denoted as B), the Scherrer's constant of 0.9 (K), the wavelength of 0.15406 nm (λ), and the half value from the 2θ peak position using the data from the XRD measurement (θ), is given by Debye Scherrer's equation: $D = K\lambda/B\cos\theta$ [23]. Additionally, the data set in XRD enables speculation of strain (ε) in the crystal lattice using the Williamson-Hall formula: $\varepsilon = (\beta\cos\theta)/(4\sin\theta)$, where β is the peak broadening [24].

3. RESULTS AND DISCUSSION

The optical properties of 4 different specimens were measured in the range of 300 – 800 nm, as depicted in Fig. 3 a. Observed that the intensity of the light transmission graphs was reduced, and the E_g was also decreased after adding rGO. Generally, the band gaps of pristine TiO_2 and SiO_2 layers are reported to be in the ranges of 3.20 – 4.04 eV and 3.85 – 8.30 eV, respectively [25]. In this work, the E_g of Tr, Tr + dip, Tr/Sr, and Tr/(Sr + dip) were obtained at 3.43 eV, 3.31 eV, 3.28 eV, and 3.25 eV, respectively, as depicted in Fig. 3 b. Herein, the changing E_g might be influenced by the effect of the ordering deposition of ETL and by incorporating rGO into ETL.

Moreover, the pivotal parameter results enable the justification of the electrical properties of 4 different specimens, like the conductivity (σ), resistivity (ρ), mobility (n), charge concentration (μ), as illustrated in Fig. 4. To clarify the pivotal parameters derived from the Hall effect measurement at room temperature for all specimens, as tabulated in Table 1.

Table 1. Pivotal parameters for the evaluation of the electrical properties at room temperature using the Hall effect equipment

Condition	$\sigma\times10^{-4}$, S/cm	$\rho\times10^{3}$, Ω/cm	$n\times10^{2}$, $cm^2/V\cdot s$	$\mu\times10^{14}$, $1/cm^3$
T	6.74	1.48	0.36	1.16
Tr	87.00	0.12	3.91	4.14
Tr +dip	188.00	0.18	5.63	7.99
Tr/Sr	44.30	0.23	1.36	2.04
Tr/(Sr + dip)	604.00	0.02	9.09	18.3

Either the incorporation of rGO in the TiO_2 and SiO_2 layers or the organization of the order of fabrication of ETL are significantly affected the σ, leading to the improvement of the electrical properties of the ETLs. For example, the σ value of the TiO_2 and SiO_2 layers can be improved after adding rGO by three orders when compared to the σ value of both layers, which have been reported before by certain research groups to be approximately 10^{-7} S/cm [8, 13]. Also, the composite of rGO into TiO_2 has been suggested to reinforce σ, reaching up to 188.3×10^{-4} S/cm using spin coating techniques [26].

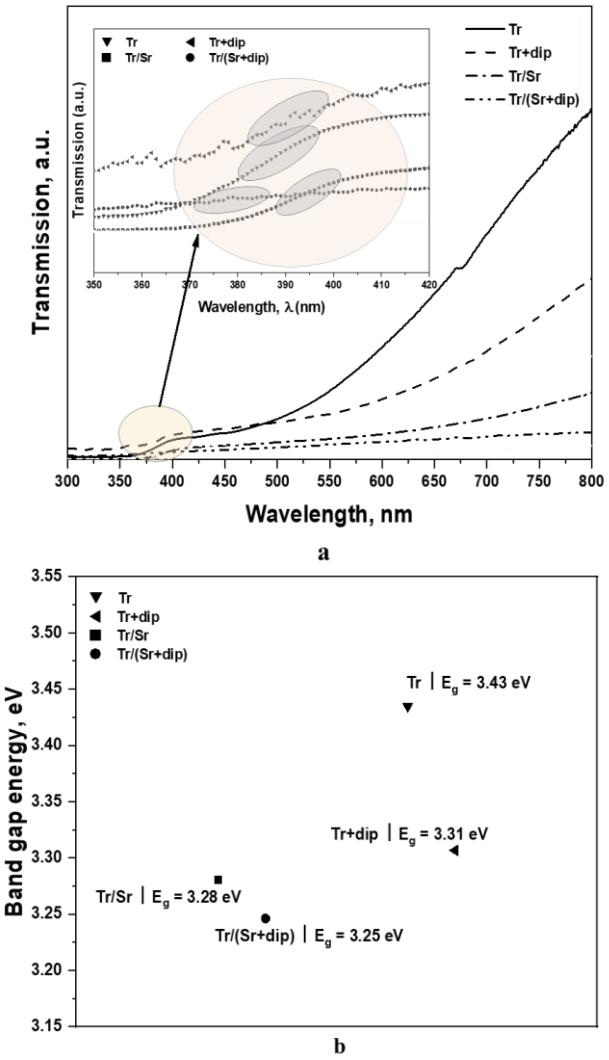

Fig. 3. a – the transmission graphs of 4 different conditions. The inset depicts the range of the light absorption edge (marked with an ellipse) that is used to calculate the E_g; b – the presentation of the E_g of all specimens

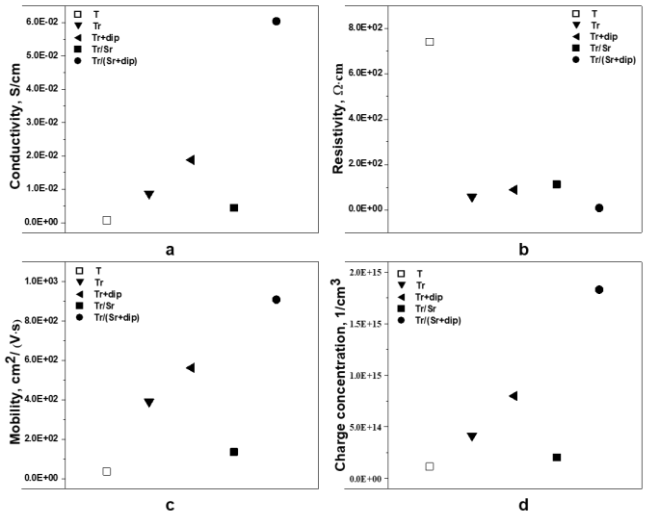

Fig. 4. The electrical parameters for 4 different specimens and the T layer: a – conductivity; b – resistivity; c – mobility; d – charge concentration

While the management of the sequential deposition of ETLs in this work, along with adding rGO into ETL, can boost the conductivity of ETLs up to 604 × 10^{-4} S/cm for the production of a dual-layer in the condition of the Tr/(Sr + dip) using the dipping approach. To confirm this wonderful result, the investigations of morphology for these specimens should be scrutinized.

Testing the morphology of these specimens can be analyzed using the XRD technique, and evaluating the significant 2θ. In this work, critical 2θ of 25.9°(101), 38.3°(004), 48.6°(200), 52.0°(105), and 62.0°(204) were ascertained and are used for the determination of the gain size (D), as demonstrated in Fig. 5 [27].

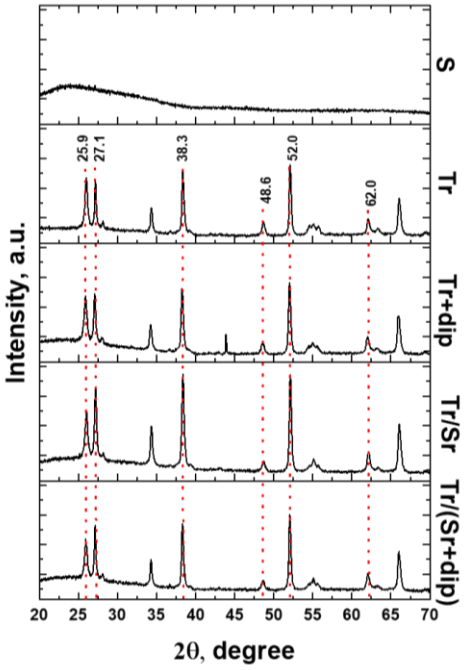

Fig. 5. The XRD pattern for S, Tr, Tr+dip, Tr/Sr, and Tr/(Sr + dip) layers

Among all the selected samples, different-width peaks have been observed, indicating that the morphology of ETL has been affected by strategies of ordered deposition of each ETL and the incorporation of rGO into ETL. The estimations of D for both rGO-doped single layer and dual-layer were noticed as 6.02 ± 0.15 nm for Tr, 15.13 ± 0.39 nm for Tr + dip, 11.67 ± 0.22 nm for Tr/Sr, and 15.95 ± 0.06 nm for Tr/(Sr + dip), respectively, as presented in Fig. 6 a.

Furthermore, the lattice distortion, as known strain in the lattice (ε), is used to elucidate the changed morphology of ETL through using information from the XRD pattern. Observed that the ε values are significantly changed after fabricating suitable dual-layer and composited rGO into ETL, as demonstrated in Fig. 6 b. Especially, the lowest ε of 0.053 for the Tr/(Sr + dip) was satisfactorily attained, which further significantly corresponds to the larger grain size.

Thus, the influence of suitable ordered deposition of dual layer and rGO incorporation into each ETL has led to a larger grain size and reduced ε, which has facilitated electron drift. A surprisingly higher conductivity was achieved through a straightforward electron transport conductive pathway, resulting in the best quality of electrical properties in this study.

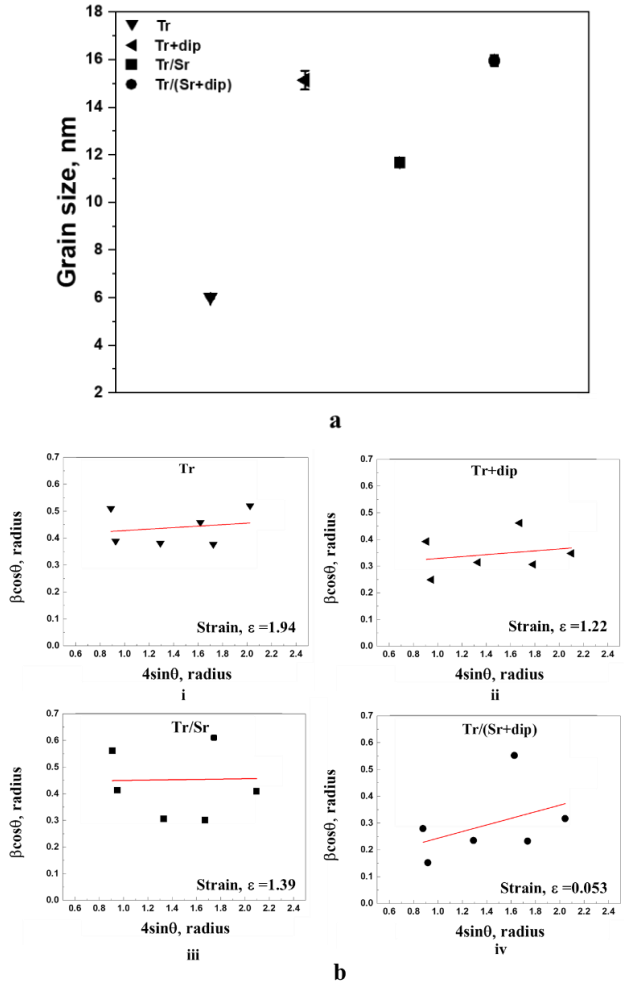

Fig. 6. a – the grain size of all specimens; b – the strain in the lattice: i – Tr; ii – Tr + dip; iii – Tr/Sr; iv – Tr/(Sr + dip)

4. CONCLUSIONS

In brief, the elevated potential of the ETL in this work is comprised of two strategies: 1) a dual layer using optimization of arranged deposition of each ETL, and 2) adding rGO into the ETL. These strategies not only enhanced the quality of the ETL, but the lattice morphology of the ETL has also undergone significant changes.

The Hall-effect measurement enables the revelation and extraction of the critical parameters of 4 different specimens in this experiment. The optimized conductivity has been validated at 604 × 10^{-4} S/cm, corresponding to a declined strain of 0.053 for the Tr/(Sr + dip) dual-layer, indicating that the ETL was improved when compared with the pristine ETL. Ultimately, a Tr/(Sr + dip) dual-layer on ETL coating fabrication using the ordered dipping process and doping with rGO was successfully attained, which can aid in boosting solar cells or building materials in the future.

Acknowledgments

The author would like to express sincere gratitude to Xi'an International University (XAIU), China, for providing financial support through the Initiation Funds for High-level

Talents Program of Xi'an International University (grant no. XAIU202521), which enabled the successful completion of this research.

REFERENCES

1. **Fatima, Q., Haidry, A. A., Zhang, H., El Jery, A., Aldrdery, M.A**. Critical Review on Advancement and Challenges in Using TiO_2 as Electron Transport Layer for Perovskite Solar Cell *Materials Today Sustainability* 27 2024: pp. 100857. https://doi.org/10.1016/j.mtsust.2024.100857
2. **Marcelis, E.J., ten Elshof, J. E., Morales-Masis, M.** Titanium Dioxide: A Versatile Earth-Abundant Optical Material for Photovoltaics *Advanced Optical Materials* 12 (36) 2024: pp. 2401423. https://doi.org/10.1002/adom.202401423
3. **Dkhili, M., Lucarelli, G., De Rossi, F., Taheri, B., Hammedi, K., Ezzaouia, H., Brunetti, F., Brown, T.M.** Attributes of High-Performance Electron Transport Layers for Perovskite Solar Cells on Flexible PET Versus on Glass *ACS Applied Energy Materials* 5 (4) 2022: pp. 4096 – 4107. https://doi.org/10.1021/acsaem.1c03311
4. **Vanaraj, R., Murugesan, V., Rathinam, B.** The Role of Optimal Electron Transfer Layers for Highly Efficient Perovskite Solar Cells-A Systematic Review *Micromachines (Basel)* 15 (7) 2024: pp. 859. https://doi.org/10.3390/mi15070859
5. **Hossain, M.K., Toki, G.F.I., Kuddus, A., Rubel, M.H.K., Hossain, M.M., Bencherif, H., Rahman, M.F., Islam, M.R., Mushtaq, M.** An Extensive Study on Multiple ETL and HTL Layers to Design and Simulation of High-Performance Lead-Free $CsSnCl_3$-Based Perovskite Solar Cells *Scientific Reports* 13 (1) 2023: pp. 2521. https://doi.org/10.1038/s41598-023-28506-2
6. **Maleki, J., Shahrostami, M., Huang, S., Abdi-Jalebi, M.** Efficiency Boost in Perovskite Solar Cells via TiO_2 Nanodiscs Embedded in The $MoSe_2$ Electron Transport Layer Revealed by Optoelectronic Simulations *Sustainable Energy & Fuels* 9 (7) 2025: pp 1797 – 1811. http://dx.doi.org/10.1039/D4SE01414F
7. **Srivastava, K.V., Srivastava, P., Srivastava, A., Maurya, R.K., Singh, Y.P., Srivastava, A.** 1D TiO_2 Photoanodes: A Game-Changer for High-Efficiency Dye-Sensitized Solar Cells *RSC Advances* 15 (7) 2025: pp. 4789 – 4819. http://dx.doi.org/10.1039/D4RA06254J
8. **Gries, T.W., Regaldo, D., Köbler, H., Putri Hartono, N.T., Harvey, S.P., Simmonds, M., Frasca, C., Härtel, M., Sannino, G.V., Félix, R., Hüsam, E., Saleh, A., Wilks, R.G., Zu, F., Gutierrez-Partida, E., Iqbal, Z., Loghman Nia, Z., Yang, F., Delli Veneri, P., Zhu, K., Stolterfoht, M., Bär, M., Weber, S.A., Schulz, P., Puel, J.B., Kleider, J.P., Unger, E., Wang, Q., Musiienko, A., Abate, A.** Co-Doping Approach for Enhanced Electron Extraction to TiO_2 for Stable Inorganic Perovskite Solar Cells *Small Science* 5 (7) 2025: pp. 2400578. https://doi.org/10.1002/smsc.202400578
9. **Yepuri, V., Rajayya, M.** Advancements in Visible Reflection Coatings: Thin Films for Photonic and Optoelectronic Applications *IEEE Photonics Technology Letters* 37 (13) 2025: pp. 729 – 732. https://doi.org/10.1109/LPT.2025.3563312
10. **Lee, S.H., Lee, J.M., Oh, J., Oh, J., Kwon, M., Park, B., Kim, W.H.** Atomic Layer Deposition of Selective SiO_2 Thin Films Using Silane Self-Assembled Monolayers on Silicon Versus Amorphous Carbon *Materials Letters* 396 2025: pp. 138749. https://doi.org/10.1016/j.matlet.2025.138749
11. **Jaroenworaluck, A., Pijarn, N., Kosachan, N., Stevens, R**. Nanocomposite TiO_2–SiO_2 Gel for UV Absorption *Chemical Engineering Journal* 181 2012: pp. 45 – 55. https://doi.org/10.1016/j.cej.2011.08.028
12. **Mursal, M., Ismail, I., Irhamni, G.** The Characteristics of Silica Nano-powder and Thin Films Prepared from Rice Husk Ash *Journal of Physics: Conference Series* 1120 2018: pp. 012039. https://doi.org/10.1088/1742-6596/1120/1/012039
13. **Muller, D., Pinheiro, G., Bendo, T., Gutiérrez Aguayo, A., Barra, G., Rambo, C.** Synthesis of Conductive PPy/SiO_2 Aerogels Nanocomposites by In Situ Polymerization of Pyrrole *Journal of Nanomaterials* 2015 2025: pp. 1 – 6. https://doi.org/10.1155/2015/658476
14. **Joshi, A.S., Elamurugu, E., Leela, S.** Impact of Graphene oxide (GO) and Reduced Graphene Oxide (rGO) on The TiO_2 Thin Film Composite (TiO_2: GO/ rGO) Photoanodes *Chemical Physics Impact* 9 2024: pp. 100667. https://doi.org/10.1016/j.chphi.2024.100667
15. **Butsriruk, K.** Optimization of rGO content in MAI:$PbCl_2$ Composites for Enhanced Conductivity *Science and Engineering of Composite Materials* 32 (1) 2025: pp. 250056. https://doi.org/10.1515/secm-2025-0056
16. **Butsriruk, K.** Design and Fabrication of Perovskite Solar Cells for Tandem Structures, Thailand, 2021: pp. 28 – 31. https://doi.org/10.58837/chula.the.2021.321
17. **Xiang, L., Yang, X., Liu, X., Fu, Z., Liu, J., Hou, T., Gou, Y., Zhao, P., Sun, X., Zhang, P.** Dip-Coating of Self-Assembled Monolayers for Perovskite Photovoltaic Applications *EcoEnergy* 3 2025: pp. e70007. https://doi.org/10.1002/ece2.70007
18. **Azarov, A., Hallén, A., Radamson, H.H.** Electrical Characterization of Semiconductors: I–V, C–V and Hall Measurements *In Analytical Methods and Instruments for Micro- and Nanomaterials*, Radamson, H.H., Hallén, A., Sychugov, I., Azarov, A. Eds.; Springer International Publishing 2023: pp. 197 – 240.
19. **Butsriruk, K., Taychatanapat, T., Chatraphorn, S.** Effects of Anti-Solvent in The Two-Step Fabrication of Absorber Layer in Perovskite Solar Cells *Journal of Physics: Conference Series* 1380 (1) 2019: pp. 012046. https://doi.org/10.1088/1742-6596/1380/1/012046
20. **Sakr, M., Liu, S.A** Comprehensive Review on Applications of Ohmic Heating (OH) *Renewable and Sustainable Energy Reviews* 39 2014: pp. 262 – 269. https://doi.org/10.1016/j.rser.2014.07.061
21. **Frank-Rotsch, C., Dropka, N., Rotsch, P.** 6 - III Arsenide *In Single Crystals of Electronic Materials*, Fornari, R. Ed.; Woodhead Publishing 2019: pp. 181 – 240.
22. **Ungár, T., Tichy, G., Gubicza, J., Hellmig, R.J.** Correlation between Subgrains and Coherently Scattering Domains *Powder Diffractio* 20 (4) 2025: pp. 366 – -375. https://doi.org/10.1154/1.2135313
23. **Bhattacharjee, P.R.** Discovery of The Lack of Success of Bragg's Law in Respect of Perfect Quantification of The X-ray Diffraction Phenomenon *Next Research* 2 (2) 2025: pp. 100312. https://doi.org/10.1016/j.nexres.2025.100312

24. **Golabiazar, R., Qadir, G.S., Faqe, Z.A., Khalid, K.M., Othman, K.I., Rasool, N.F., Saeed, H.F.** Green Biosynthesis of CdS NPs and CdS/Fe_3O_4 NCs by Hawthorn Plant Extract for Photodegradation of Methyl Orange Dye and Antibacterial Applications *Journal of Cluster Science* 33 (3) 2022: pp. 1223 – 1238. https://doi.org/10.1007/s10876-021-02054-z

25. **Bayazıt, T., Kanmaz, İ., Tomakin, M., Üzüm, A.** Triple layer $TiO_2/HfO_2/SiO_2$ Thin Film Design for Reduction of Optical Losses *Physica Scripta* 2025: pp. 45949. https://doi.org/10.1088/1402-4896/adc049

26. **Rafidah, K., Siti, K.S., Afiqah, B.**The Effects of Annealing Temperature Dependence on the Doping of Titanium Dioxide (TiO_2) and Reduced Graphene Oxide (rGO) for Perovskite Solar Cell Application *International Journal of Nanoelectronics and Materials* 13 (3) 2020: pp. 421 – 432. http://ir.unimas.my/id/eprint/33248

27. **Morad, I., El-Desoky, M.M., Mansour, A., Wasfy, M.** Synthesis, Structural and Electrical Properties of PVA/TiO_2 Nanocomposite Films with Different TiO_2 Phases Prepared by Sol-Gel Technique *Journal of Materials Science Materials in Electronics* 27 2024: pp. 17574 – 17584. https://doi.org/10.1007/s10854-020-04313-7